Nuclear Instruments and Methods in Physics Research A 600 (2009) 506–512

Contents lists available at ScienceDirect

Nuclear Instruments and Methods in Physics Research A

journal homepage: www.elsevier.com/locate/nima

# GEANT4 studies on the propagation and detection of scintillation light in long thin YAP crystals

F. Ciocia [a], A. Braem [b], E. Chesi [b], R. De Leo [a,*], C. Joram [b], L. Lagamba [a], E. Nappi [c], J. Séguinot [b], I. Vilardi [a], P. Weilhammer [b]

[a] Physics Department and INFN Section of Bari, Via Orabona 4, Bari, Italy
[b] CERN PH-Department, CH-1211 Geneva, Switzerland
[c] INFN Section of Bari, Via Orabona 4, Bari, Italy

ARTICLE INFO

*Article history:*
Received 18 February 2008
Received in revised form
24 November 2008
Accepted 30 November 2008
Available online 7 December 2008

*Keywords:*
GEANT4
YAP:Ce
Molecular imaging
PET

ABSTRACT

The response to γ-rays of long thin polished or wrapped YAP:Ce scintillator bars read out at both edges by photomultipliers has been studied by means of GEANT4 simulations with the aim to investigate the capability of the charge division method to reconstruct the gamma interaction point in the crystal. The GEANT4 simulations took into account the optical properties of the scintillator like absorption, reflection, and diffusion during the passage of the light through the crystal. The simulations were able to reproduce experimental measurements of light yields in polished and wrapped YAP:Ce crystals with dimensions $3.2 \times 3.2 \times 100\,mm^3$. Once validated, the simulations could show that a particular patterning of the crystal surface, which enhances the surface absorption, should lead to a significant improvement of the reconstruction precision of the charge division method, without compromising the energy resolution.



## 1. Introduction

The availability of "long thin" inorganic scintillators [1], shaped either as bars or fibers, bundled to arrays and read out at both ends by pixelized photodetectors, opens new perspectives in medical gamma ray detection, both for non-invasive diagnosis and monitoring systems.

In 2006, a Positron Emission Tomography (PET) device was proposed [2] based on axially oriented arrays [3] of long (10–15 cm) and thin (4–9 $mm^2$) polished or wrapped scintillator bars read out at both ends [3,4] by pixelized photodetectors [5]. A schematic view of an array of such a device is shown in Fig. 1. This novel "axial PET concept" [2] promises parallax-free 3D reconstruction of the γ-ray interaction point, as the third coordinate, i.e. the axial $z$-coordinate, is derived from the ratio of the amounts of light detected at the two crystal ends. The resolution in the transverse ($x$–$y$) coordinates is given by the (squared) crystal bar width $d$: $\sigma_{x,y}=d/\sqrt{12}$. Although recently an alternative and potentially more accurate approach for the axial coordinate was proposed [6], the light-sharing method could still be an interesting and powerful method for position reconstruction in PET devices, as well as in other possible (non-medical) applications.

The resolutions of the axial $z$-coordinate ($\sigma_z$) and of the gamma ray energy ($\sigma_E/E$) in "long thin" scintillators are driven [2,7], as shown in Section 2, by two key parameters: $\lambda_{eff}$ and $N_0$. The effective light absorption length, $\lambda_{eff}$, describes the absorption of scintillation photons on their path through the crystal bulk and at the crystal borders. $N_0$ is the number of photoelectrons ($pe$'s) that would be detected in a fully transparent crystal bar ($\lambda_{eff}=\infty$) following the conversion of a 511 keV γ-ray. The $\lambda_{eff}$ and $N_0$ values depend on both the physical and optical properties of the chosen scintillator and its lateral surface [2,7], and on the characteristics of the photodetectors.

A recent experimental study [7], carried out on a set of polished YAP:Ce scintillators of dimensions $3.2 \times 3.2 \times 100\,mm^3$, demonstrated the possibility of adjusting $\lambda_{eff}$ by wrapping [8] the bar's lateral surfaces with Teflon or by coating these surfaces with very thin metallic layers.

In this paper, we present the results of Monte Carlo simulations of the optical processes involved in the propagation and detection of the scintillation light from the crystal bars. The package GEANT4 has been used [9] and the results of the simulations have been subsequently compared with previously published experimental measurements [7]. The understanding of the influence of the optical properties of the crystal surfaces on the light collection is fundamental to optimize the performance of a long thin scintillator.

The low effective $Z$ of YAP:Ce leads also to a low photofraction [2] which makes it unsuitable for a PET device. However, the

*Corresponding author. Tel.: +39 080 5443242; fax: +39 080 5534938.
*E-mail address:* deleo@ba.infn.it (R. De Leo)

0168-9002/$ - see front matter © 2008 Elsevier B.V. All rights reserved.
doi:10.1016/j.nima.2008.11.133

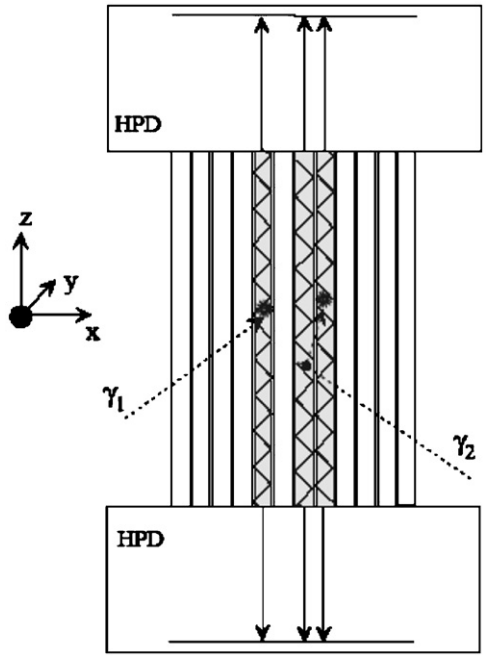


**Fig. 1.** 3D axial PET concept [2]. Schematic view of one detector module. Matrices of axially arranged long crystals are read out on both edges by segmented photodetectors (HPDs [5]).

availability of accurate data [7] led to the decision to focus the simulation studies presented in this article on this scintillator material.

The present paper is organized as follows: Section 2 discusses the analytical expressions for the spatial and energy resolutions of a long thin scintillator bar as a function of the main parameters. Section 3 gives a condensed summary of the experimental results previously published in [7]. The GEANT4 simulations and their results are presented in Section 4, together with a discussion on their dependence on the main optical parameters. The conclusions of the paper are summarized in Section 5.

## 2. Energy and axial resolutions in a long thin crystal

In a long ($L_C$) and thin crystal the photoelectric yields $N_1(z)$ and $N_2(z)$ measured by the two photodetectors at the bar ends are modeled as exponential functions with their distance from the interaction point ($z$) of the $\gamma$-ray (see Fig. 2), calculated with the following expressions:

$$N_1(z) = \frac{1}{2} N_0 \exp\frac{-z}{\lambda_{eff}}, \quad N_2(z) = \frac{1}{2} N_0 \exp\frac{-(L_C - z)}{\lambda_{eff}} \tag{1}$$

$$N_{pe}(z) = N_1 + N_2 \tag{2}$$

with $N_{pe}$ being the total number of detected photoelectrons. $\lambda_{eff}$ is smaller than the crystal bulk absorption length $\lambda_{bulk}$ as it is related to the effective scintillation photon path length inside the crystal.

The expression for the axial $z$-coordinate of the interaction point is derived using the light division method [2,3]:

$$z = \frac{1}{2}\left(\lambda_{eff} \ln\frac{N_2}{N_1} + L_C\right) \tag{3}$$

The uncertainty on the reconstructed $z$-coordinate, ignoring any uncertainty in the knowledge of $\lambda_{eff}$ ($\sigma(\lambda_{eff}) = 0$), and taking into account only the statistical error of $N_{1,2}$, ($\sigma(N_{1,2}) = \sqrt{ENF \cdot N_{1,2}}$), is given by

$$\sigma_z = \frac{\lambda_{eff}}{2}\left[\frac{\sigma^2(N_2)}{N_s^2} + \frac{\sigma^2(N_1)}{N_1^2}\right]^{1/2} = \frac{\lambda_{eff}}{\sqrt{2N_0/ENF}}\left(\exp\frac{z}{\lambda_{eff}} + \exp\frac{L_C - z}{\lambda_{eff}}\right)^{1/2}. \tag{4}$$

The energy resolution is

$$\frac{\sigma_E}{E} = \sqrt{\frac{ENF}{N_{pe}} + R_{\text{int}}^2}. \tag{5}$$

In the previous equations, $ENF$ is the excess noise factor of the photodetector [2,5], and $R_{int}$ the intrinsic (non-statistical) resolution of the scintillator [10].

These equations clearly imply that an increase in $N_0$ results in an improvement of both the axial and energy resolutions. On the other hand, an increase of $\lambda_{eff}$ improves $\sigma_E/E$ but has an adverse effect on $\sigma_z$. The dependences of $\sigma_E/E$ and $\sigma_z$ on $\lambda_{eff}$ have been experimentally verified (see Fig. 11 of Ref. [7]). The best compromise for the choice of $\lambda_{eff}$ was predicted by the simulations in Ref. [2] to be about 2/3 of the crystal length $L_C$.

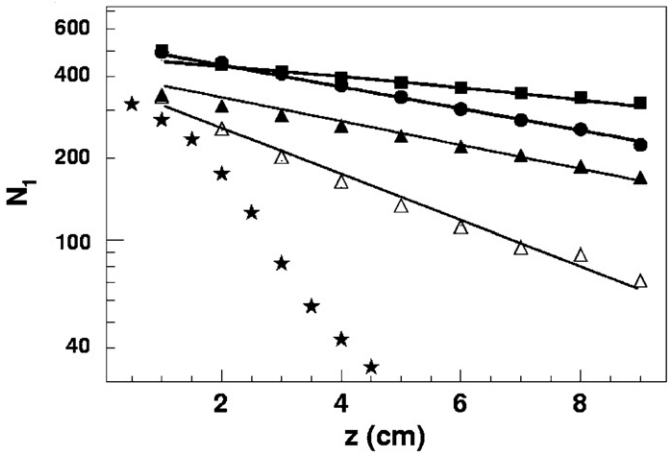


**Fig. 2.** Photoelectric yield at the photopeak, measured with a PMT H3164-10 for 511 keV $\gamma$-rays impinging laterally on a 10 cm long YAP crystal at various $z$-positions. The experimental points, taken from Ref. [7], are for a polished crystal (filled squares), a Teflon wrapped crystal (filled points), a crystal coated with 1 nm Cr (filled triangles), a crystal coated with 1.5 nm Au (empty triangles). Stars refer to a 5 cm YAP crystal with the lateral surface roughened and wrapped with Teflon. The lines are fits to simulated data (not shown for clarity) based on Eq. (1). The deduced parameters $N_0$ and $\lambda_{eff}$ are reported in Table 1.

## 3. Experimental results

Fig. 2 shows a set of measurements performed with polished 10 cm long YAP crystal bars of $3.2 \times 3.2\,mm^2$ cross-section, with lateral surfaces which had undergone various treatments [7].

An effective light absorption length of 20.8 cm was measured for polished YAP crystals in air (filled squares in Fig. 2), i.e. a factor of about three higher than the optimum value suggested by the simulations in Ref. [2]. The axial resolution ($\sigma_z$) was found to be 8 mm (full squares in Fig. 3). The energy resolution in the centre of the bar was found to be 4.6% (at $E_\gamma$=511 keV).

Teflon wrapping (filled points in Fig. 2) did not degrade the parameter $N_0$ with respect to a polished crystal [the $N_0$ value can be extracted from the $N_1$ values in Fig. 2, considering that $N_0 \sim 2 \cdot N_1(z{=}0)$]. The only effect of the wrapping was to diminish $\lambda_{eff}$ by a factor of 2. Hence, as expected from Eq. (4), the $\sigma_z$ resolution improved (filled points in Fig. 3).

$\lambda_{eff}$ could be tuned with metallic coatings (triangles in Fig. 2) in the range from 11.9 to 3.9 cm [7] by adjusting the thickness of the coatings in the range of a few nanometers. However, absorption of the metal films (their refractive index is complex) led to unacceptably large losses in the collected light.

A very low $\lambda_{eff}$ value (~1.5 cm) could be obtained by roughing the crystal lateral surface with sand paper (stars in Fig. 2). However, detection of correlated signals at the two scintillator ends which exceeded a threshold of 30 keV (equivalent to polished surfaces) was only possible with a shorter ($L_C$=5 cm) sanded and Teflon wrapped crystal. Moreover, the exponential $z$-dependence of the *pe* yield was lost except in the central part of the crystal.

All experimental data in Figs. 2 and 3 refer to the photopeaks produced by 511 keV γ-rays.

## 4. GEANT4 simulations

We discuss in this section the optical and geometric parameters implemented in the GEANT4 simulations to describe the light collection and photoelectron production. Their influence on the $\sigma_z$, and $\sigma_E/E$ resolutions is analysed on the basis of the experimental results shown in the previous section. We show that, once validated with experimental data, the GEANT4 code provides an efficient tool for searching the most appropriate technique to achieve the optimum performance of a long thin scintillator bar.

### 4.1. Principle and validation of the simulations

Simulations were performed with the Monte Carlo code GEANT4 [9]. A YAP scintillator bar with a square cross-section ($3.2 \times 3.2\,mm^2$) was implemented. The following intrinsic properties of the scintillator were assumed [2]: bulk absorption length $\lambda_{bulk}$=24 cm (corresponding in polished crystal to the measured effective absorption length of 20.8 cm), light yield $N_{ph}$=18/keV, intrinsic energy resolution $R_{int}$=2.4%, refractive index $n_1$=1.94. The crystal lateral surface was assumed to be either polished and surrounded by air, or fully or partially (fraction $f_2$ in Table 1) wrapped with a material characterized by its refractive index $n_2$ (for Teflon, $n_2$=1.3). Studies were also performed with the bar assumed to be completely ($f_2$=1) coated by a metal film. In this case the film of thickness $t$ was characterized by its complex refractive index $n_2$, $k_2$ (Cr: $n_2$=1.87, $k_2$=2.69; Au: $n_2$=1.7, $k_2$=1.88). The two photodetectors coupled to the crystal polished end faces were assumed to be photomultipliers (PMTs), with characteristics similar to the PMTs used in [7]: a borosilicate window with refractive index $n_w$=1.474, an *ENF* value of 1.2, and a quantum efficiency $\varepsilon_Q$=0.25.

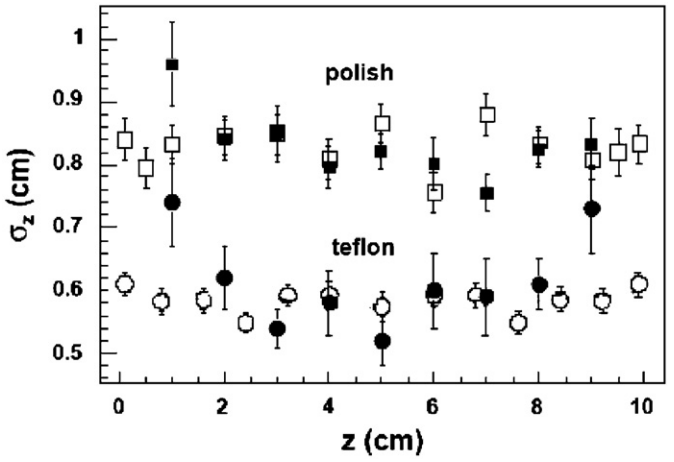


**Fig. 3.** Uncertainties in the reconstructed scintillation position ($\sigma_z$, standard deviations of the reconstructed $z$-distributions), as a function of the $z$-position, for a polished and a Teflon wrapped YAP crystal. The open symbols represent the results of the simulations, while the filled symbols show experimental results.

γ-Rays of 511 keV impinged perpendicularly on the crystal lateral surface, at a fixed $z$-position. To minimize the computational time, only photoelectric interactions were considered. Events in which the energy was released in a cascade (Compton scattering, followed by photoelectric effect) were not considered in the present simulations. These events occur with a low probability, due to the small transverse dimensions of the crystal. GEANT4 randomly chooses the number of optical photons generated by each γ-ray in a Gaussian centred on the light yield ($511\,keV \cdot N_{ph}$) with a width proportional to the quadratic sum of the statistical uncertainty and the crystal intrinsic resolution. The optical scintillation photons were generated with an isotropic distribution. The optical dispersion of the various materials in the wavelength band of the scintillation light was ignored, however the refractive indices of the various materials and the photocathode quantum efficiency were assumed to be those at the wavelength of maximum emission of YAP:Ce (370 nm). Only the absorption ($\lambda_{bulk}$) process was considered when tracking optical photons inside the crystal. For photons arriving at the lateral crystal surfaces, the following processes were considered (see Fig. 4), in agreement with the model in [11]: absorption ($A$), diffusion ($D$), modelled with a Lambertian distribution, transmission ($T_S$) and reflection ($R_S$). These distributions have an angular smearing ($S$). The normal to the local surface is rotated with respect to the average crystal surface by a polar angle randomly chosen from a Gaussian distribution with average 0 and width $\sigma_\alpha$. Obviously, the sum of the probabilities $P(A)+P(D)+P(R_S)+P(T_S)$ is normalized to 1. The reflection and transmission probabilities ($R_S$ and $T_S$) [or simply $T$ and $S$ when $\sigma_\alpha$=0, $P(R_S)+P(T_S)=P(R)+P(T)$], were calculated according to the Fresnel relations assuming random polarization of the incident photons. When the transmission process was selected, the photon was considered lost and no longer tracked, except if the crystal was coated with a film. In the latter case, the photon was followed in the coating. Here the photon could either get absorbed or fully traverse the coating (in both cases the photon was lost) or bounce back into the crystal.

A polished crystal in air was described by $n_2=n_{air}$=1, $\sigma_\alpha=D=A$=0. For a partially diffusive wrapping with refractive index $n_2$ we

**Table 1**
Values of the parameters $N_{ph}$, $A$, $D$ and $f_2$ used in the GEANT4 simulations represented in Figs. 2 and 3.

| Wrap | $N_{ph}$ ($keV^{-1}$) | $A$ (%) | $D$ (%) | $f_2$ | $N_0$ (*pe*) (Fig. 2) | $\lambda_{eff}$ (cm) (Fig. 2) | $N_0$ (*pe*) (Fig. 3) | $\lambda_{eff}$ (cm) (Fig. 3) |
|---|---|---|---|---|---|---|---|---|
| Polish | 22.5 | 0 | 0 | 0 | 963 | 21.1 | 1052 | 21.8 |
| Teflon | 22.5 | 0.3 | 2 | 0.5 | 1062 | 10.8 | 1124 | 13.9 |
| Cr | 22.5 | 0 | 0 | 1 | 820 | 9.9 | | |
| Au | 22.5 | 0 | 0 | 1 | 767 | 5.1 | | |

The values of the parameters $N_0$ and $\lambda_{eff}$ were derived from the fits of the simulations in Figs. 2 and 3 with Eqs. (1) and (4), respectively.

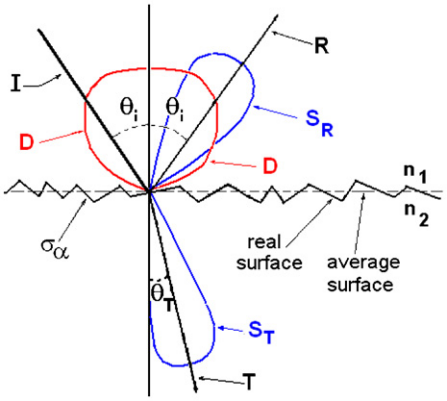


**Fig. 4.** Schematic representation of the possible processes at the interface between the crystal ($n_1$) and the coated (or wrapped) lateral surface ($n_2$). Absorption ($A$) is not indicated. The figure has been adapted from Fig. 3 of Levin et al. [11].

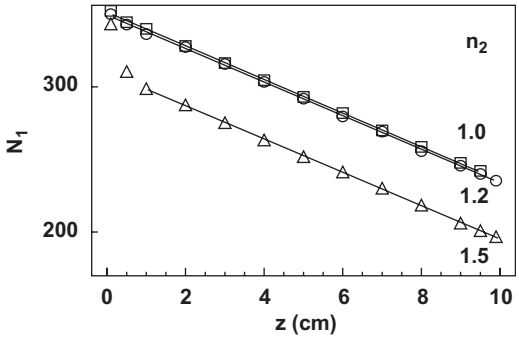


**Fig. 5.** Simulated number of photoelectrons $N_1$ detected at one end of the crystal bar, for scintillation occurring at various $z$-positions in a YAP crystal, with the lateral surfaces polished (circles), or wrapped with the indicated refractive indices ($n_2$=1.2 squares, $n_2$=1.5 triangles). The PMT was assumed to be equipped with a borosilicate window ($n_w$=1.474). The lines are the results of a fit based on Eq. (1).

chose $\sigma_\alpha$=0, $D\neq 0$, $A\neq 0$, and for a roughened crystal surface $n_2$=1, $\sigma_\alpha\neq 0$. For partially wrapped crystals ($f_2<1$), the lateral surface is divided in the $z$-direction with wrapped strips (with refractive index $n_2$), with width $f_2\cdot 0.5$ mm, alternated with strips of air $(1-f_2)\cdot 0.5$ mm wide. The choice of the strip size is somewhat arbitrary, it should however be small compared to the expected axial resolution.

A photon traversing the photodetector window was converted into a photoelectron with a random probability chosen in a Poisson distribution with $\varepsilon_Q$ as average value. There is also a non-zero probability for a converted photon to produce 2 or more photoelectrons.

The $N_1$ and $\sigma_z$ values were evaluated in the Monte Carlo simulations by following one thousand $\gamma$-rays impinging perpendicularly on the crystal's lateral surface at fixed positions, ranging from $z$=1 to 9 cm. A fit of the evaluated $N_1$ values to Eq. (1) is shown by the solid lines in Fig. 2. The slopes and the extrapolations to $z$=0 of these lines give, respectively, the $\lambda_{eff}$ and $N_0$ values reported in the sixth and seventh column of Table 1. The evaluated position uncertainties $\sigma_z$ are reported in Fig. 3 with open symbols. They are the standard deviations of the distributions of the reconstructed scintillation points obtained through Eq. (3) multiplied by $(ENF)^{1/2}$. Their fits to Eq. (4) give $\lambda_{eff}$ and $N_0$ values (reported in last two columns of Table 1) which are in good agreement with those deduced from the fits of the evaluated $N_1$'s according to Eq. (1).

The values of the $A$, $D$ and $f_2$ parameters used in the simulations shown in Figs. 2 and 3, are reported in Table 1. In order to reproduce the experimental results, it was necessary to adjust the light yield $N_{ph}$. The obtained value of 22.5/keV (see Table 1), is slightly higher than values reported in literature (18/keV) [2]. This observation may indicate an improved photon yield for the YAP crystals used in the experimental study of [7]. The Teflon wrapped crystal required a low percentage of Lambertian diffused photons ($D$ value), probably due to the efficient pulling of the Teflon tape during the crystal wrapping. With these values, a striking agreement is observed in Figs. 2 and 3 between the experimental data and the results of the Monte Carlo simulations, thus providing confidence in the validity of the simulations.

### 4.2. Influence of the optical parameters on $\sigma_z$ and $\sigma_E/e$

The transmission of the scintillation light to the photodetector depends on the critical angle at the interface between crystal and PMT entrance window: $\theta_a=\sin^{-1}(n_w/n_1)$.

In long thin crystal bars, the produced scintillation light which is transmitted to the photodetector can be divided into two components.

The "direct" component, which reaches the detector without reflections from the lateral crystal surfaces, is dominant for gamma interactions at short distances from the window. Its fraction is

$$f(\theta_a)=\frac{1}{4\pi}\cdot 2\pi\cdot\int_0^{\theta_a}\sin\theta\,\mathrm{d}\theta=\frac{1}{2}\cdot[1-\cos\theta_a]. \tag{6}$$

where $\theta$ is the polar angle w.r.t. the $z$-direction. The number of detected "direct" photoelectrons is

$$N_{0a}=N_{ph}\cdot f(\theta_a)\cdot\varepsilon_Q. \tag{7}$$

The "indirect" component is the fraction of photons which propagates in the crystal bar by total internal reflection. It is limited to polar angles in the range from 0 to $\pi/2-\theta_b$ with $\theta_b=\sin^{-1}(n_2/n_1)$ being the critical angle at the bar lateral surface.[1] The photoelectron yield of the "indirect" component

$$N_{0b}=N_{ph}\cdot f\left(\frac{\pi}{2}-\theta_b\right)\cdot\varepsilon_Q \tag{8}$$

decreases when $n_2$ increases, i.e. when a coating or a wrapping is used. However, for $1<n_2\leqslant 1.25$, the high $n_1$ of YAP crystals maintains the transmission at the photodetector's borosilicate window ($n_w$=1.474) as limiting factor, although the intensity of the indirect component decreases. The overall yield is therefore unchanged (see Fig. 5). On the contrary, for higher values of $n_2$ (see for example the case of $n_2$=1.5 in Fig. 5), the decrease of the indirect component becomes the dominant effect.

The behaviour is completely different with a sapphire window ($n_w$=1.793). The transmitted photon flux starts to decrease as soon as $n_2$ exceeds 1.

As can be deduced from Fig. 5, $\lambda_{eff}$ is not much dependent of $n_2$. However, at small distances, one observes a slight deviation from an exponential behaviour due to the detection of the direct component. The increase of $\sigma_z$ at the scintillator borders, observed experimentally (see Fig. 3), could be due to either an increased statistical variations in the number of photons from scintillator ends, or the non exponential rule followed by these photons.

The influence of $n_w$ on $N_1$ and $\sigma_z$ for polished crystals in air is shown in Fig. 6. Results for the refractive index of sapphire,

[1] This analytical expression is only correct for cylindrical crystals. For a rectangular crystal the accepted angular range is somewhat larger, but the argument remains fully valid.

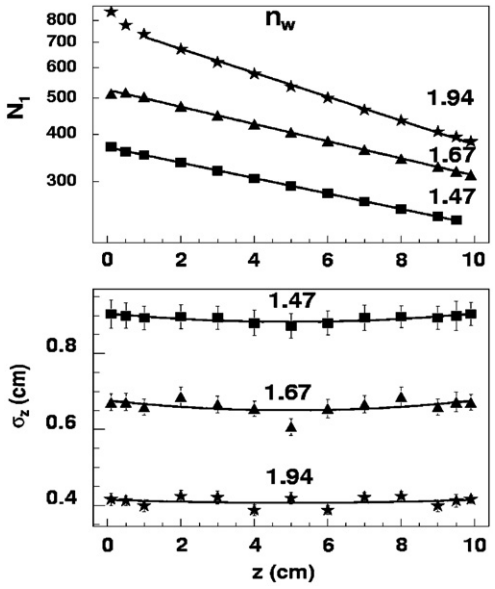


**Fig. 6.** Simulated number of photoelectrons $N_1$ detected at one bar end (upper plot) and $z$-resolutions (lower plot) for scintillation at various $z$-positions in a YAP bar. The crystal lateral surface is optically polished ($n_2$=1). The data sets correspond to photodetectors with different refractive indices of the entrance windows. The lines in the upper and lower plots are fits based on Eqs. (1) and (4) respectively.

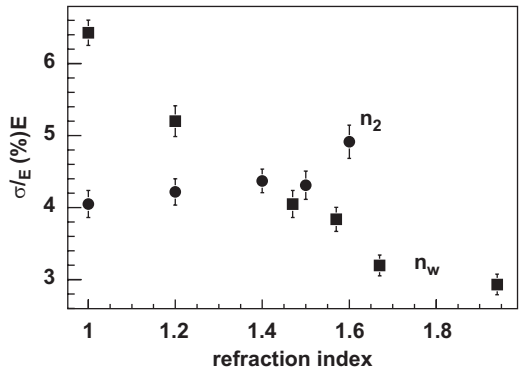


**Fig. 7.** Simulated energy resolutions for 511 keV γ-rays detected in the centre of a 10 cm long YAP crystal. The circles correspond to a variation of the refractive index ($n_2$) of the lateral surface wrapping for a borosilicate window ($n_w$=1.474). The squares represent a variation of the refractive index of the PMT entrance window ($n_w$) while $n_2$ is maintained at 1 (no wrapping).

$n_w$=1.793, are not shown, however they can easily be estimated by interpolation between the shown values $n_w$=1.67 and 1.94.

As previously mentioned, $N_0$ increases with $n_w$. The maximum value is reached when the crystal-window refractive indices are matched. A reduction of the effective attenuation length $\lambda_{eff}$ with $n_w$ is observed (upper plot of Fig. 6), which leads to a significant improvement of the $\sigma_z$ resolution (lower plot of Fig. 6).

The energy resolution of γ-rays interacting at the crystal centre ($z$=$L_C$/2=5 cm), shown in Fig. 7, worsens for increasing values of $n_2$ (filled circles), and for decreasing $n_w$ values (filled squares).

The influence of the absorption ($A$) on $N_1$ and $\sigma_z$ is displayed in Fig. 8. An increased value of the parameter $A$ does not result in a smaller $N_0$ but in a lower value for $\lambda_{eff}$. As a consequence, an improvement in $\sigma_z$ is observed, which saturates however for values of $A$ above 10%. The results in Fig. 8 are for a borosilicate window ($n_w$=1.474) and would obviously improve for a sapphire window.

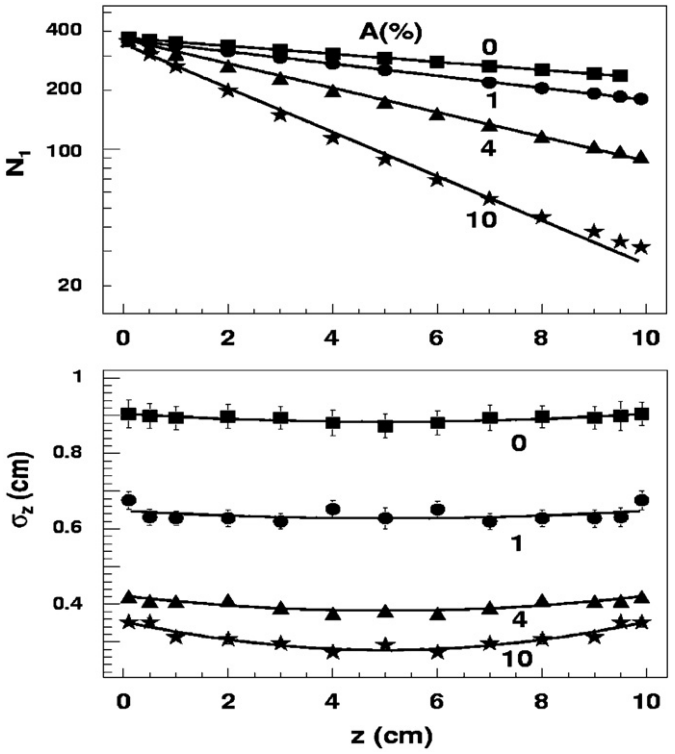


**Fig. 8.** Simulated photoelectric yield $N_1$ detected at one end of a polished bar (upper plot) with the absorption parameter $A$ varied as indicated, and for $n_2$=1 and $n_w$=1.474. Lower plot: corresponding uncertainties in the reconstructed $z$-positions.

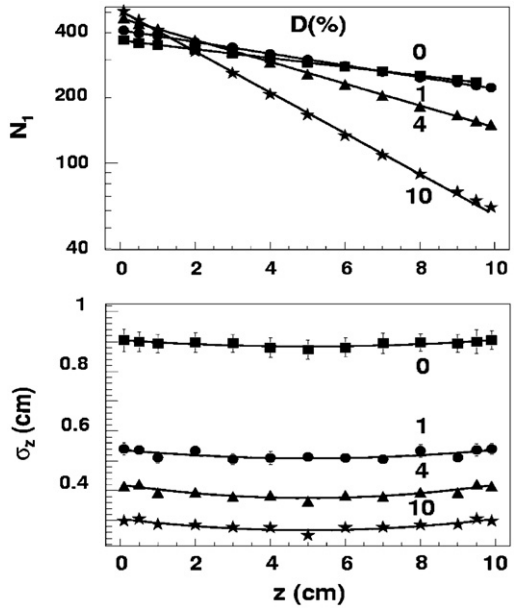


**Fig. 9.** Same as Fig. 8 for a YAP bar with the lateral surface polished ($n_2$=1) and diffusive according to the indicated percentages ($D$). The PMT entrance window was assumed to be borosilicate ($n_w$=1.474).

The influence of the diffusion parameter ($D$) on $N_1$ and $\sigma_z$ is shown in Fig. 9. The effects are similar to those of the absorption, although in this case an increase of $N_0$ for increasing values of $D$ is observed. This is caused by photons travelling with polar angles above the critical angle $\pi/2-\theta_b$, which would be lost in a polished crystal, but can be re-emitted after the diffusion process with a

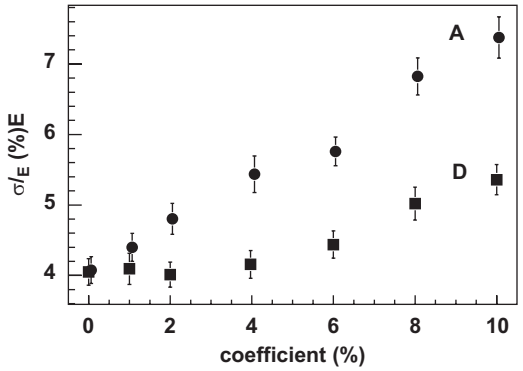


**Fig. 10.** Energy resolutions evaluated for 511 keV γ-rays at the centre of a 10 cm long YAP crystal, versus the percentages of the photon flux undergoing absorption (circles) or diffusion (squares). The results are for $n_2$=1 and $n_w$=1.474.

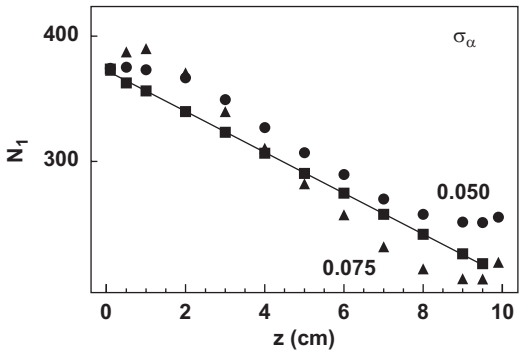


**Fig. 11.** Simulated number of photoelectrons $N_1$ detected on one bar end for scintillation at various $z$-positions in a YAP bar for a polished (squares plus fitted line) and roughened surface (circles and triangles). The typical angular smearing $\sigma_\alpha$ (in rad) is indicated. The results are for a borosilicate PMT window ($n_w$=1.474).

lower polar angle and therefore be detected. For this reason, transport efficiencies greater than those calculated with Eq. (8) can be obtained. The improvement in $\sigma_z$ due to absorption and diffusion is offset by a degradation of the energy resolution, as observed in Fig. 10, evaluated for γ-rays interacting at the crystal centre. However, the degradation is reduced for a diffusive coating due to the increase of $N_0$.

As shown in Fig. 11, the angular smearing effect destroys the exponential dependence of $N_1$ on the $z$-coordinate, and more importantly gives nearly $z$-independent $N_1$ values at the crystal borders, thus making the scintillation position reconstruction no longer possible, neither by using Eq. (3), nor by the more simple barycentre formula $z=(N_1-N_2)/(N_1+N_2)$ [1].

As expected, the $N_0$ and $\lambda_{eff}$ values were not found to vary appreciably with the crystal cross-section and length $L_C$ for polished YAP crystals when they were coupled to a PMT with a borosilicate window. However, an increase of the crystal length results in a worsening of the position resolution in agreement with Eq. (4) for a constant $\lambda_{eff}$.

The simulations suggest that a low percentage of photons undergoing Lambertian diffusion (obtainable, for example, with a partial roughening of the lateral surfaces) is a good approach to improve $\sigma_z$. However, the challenge of such a technique would be to obtain high reproducibility of the surface quality for a large number of bars.

An alternative approach, which in practice should lead to reproducible results, is to modify the geometry of the crystal such that it allows a fraction of the photons to escape through the lateral faces. Such a method could be implemented by applying triangular engravings (cuts) to the lateral surfaces of a polished

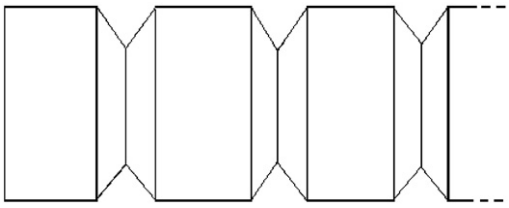

**Fig. 12.** Engravings on the lateral surface of a polished crystal (not to scale). Their number (from 10 to 100/cm) and depth (from 50 to 100 μm) can be used to tune the effective absorption of the scintillation photon propagating along the crystal.

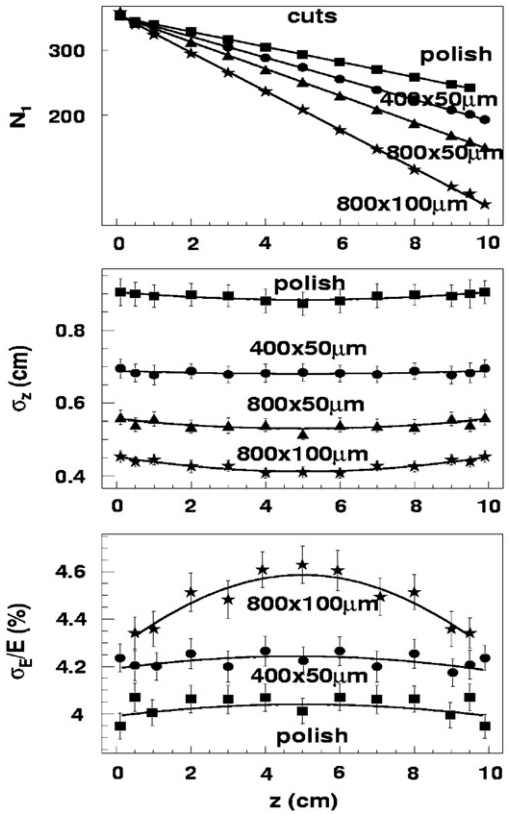


**Fig. 13.** Simulated number of photoelectrons $N_1$ (upper plot) at one bar end (photodetector with $n_w$=1.474), $z$-resolution (middle plot) and energy resolution (lower plot) as a function of the $z$-position. The lateral polished surfaces are engraved with patterns varying in number and depth of the cuts as indicated.

crystal bar (see Fig. 12). In this case, the absorption probability $A$ depends on the number of cuts and their depth. Technically, the pattern can be produced by laser etching followed by chemical polishing [12]. The effect of engravings has been simulated in the present work with GEANT4, for various patterns.

Fig. 13 illustrates the performance which can be achieved for various parameters of the engravings. The $N_1(z)$ relation can be kept perfectly exponential using this method. In contrast to all other methods it significantly improves $\sigma_z$ while leaving $\sigma_E/E$ practically unaffected. Furthermore, the resolutions are almost constant over the full bar length.

## 5. Conclusions

We presented the results of GEANT4 simulations to evaluate the spatial and energy resolutions of long thin YAP:Ce scintillator bars equipped with PMTs at the two end faces.

Previous measurements carried out on the various experimental configurations obtained by wrapping or coating the crystal lateral surface provided results for the achievable resolutions $\sigma_E/E$ and $\sigma_z$. These results are well reproduced by the GEANT4 simulations and accounted for by the parameters $N_0$ and $\lambda_{eff}$, which are the key quantities for characterizing the crystal-photodetector system.

The various optical parameters involved in the propagation of the scintillation photon flux have been identified and their respective contributions to the resolutions analysed by means of the simulations.

The simulations have shown that the detected light yield, and consequently the energy and position resolutions of the detected $\gamma$-ray can be optimized by matching the refractive indices of the crystal and photodetector windows. With borosilicate windows the simulations indicate that the most appropriate way to optimize the resolutions is to realize controlled absorption of the photons by engraving the crystal lateral surfaces using laser etching and chemical polishing.

We plan to experimentally demonstrate the effects of the engravings on YAP bars and to extend the simulations to crystals based on LYSO.

The studies presented in this article indicate that the various wrapping and coating techniques of 10 cm long YAP crystal bars can lead to a $z$-resolution of the order of $\sigma_z$=0.4 cm, i.e. a FWHM value of about 1 cm. Earlier calculations [2] indicate that the $z$-resolution can be pushed under optimized conditions to about $\sigma_z$=0.2–0.3 cm by choosing modern scintillators with higher light yield (LSO, LYSO, $LaBr_3$).

However, even with these $z$-resolutions, the charge division method in long thin crystals does not represent a clear improvement in the PET field over existing state-of-the-art devices like the HRRT scanner [13]. The alternative method proposed in [6] avoids the dilemma between optimized energy and $z$-resolution which can only be handled by a careful tuning of the effective absorption length. It allows achieving sub-millimetre $\sigma_z$ values, independent of the crystal length.

## References

[1] B. Hautefeuille, et al., J. Cryst. Growth 289 (2006) 172;
P. Anfré, et al., IEEE Trans. Nucl. Sci. NS-51 (2007) 391.
[2] J. Seguinot, et al., Novel geometrical concept of high performance brain PET scanner—principle, design and performance estimates, CERN PH-EP/2004-050, Il Nuovo Cimento, 29C (2006) 429–463 (available at: 〈http://ssd-rd.web.cern.ch/ssd-rd/Pad_HPD/Literature/pet.pdf〉).
[3] K. Shimizu, et al., IEEE Trans. Nucl. Sci. NS-35 (1988) 717.
[4] J.S. Huber, W.W. Moses, M.S. Andreaco, O. Petterson, IEEE Trans. Nucl. Sci. NS-48 (2001) 684;
E. Gramsch, R.E. Avila, P. Bui, IEEE Trans. Nucl. Sci. NS-50 (2003) 307;
P.A. Dokhale, et al., Phys. Med. Biol. 49 (2004) 4293.
[5] C. Joram, Nucl. Phys. B (Proc. Supp.) 7 (1999) 407;
E. Chesi, et al., Nucl. Instr. and Meth. A 564 (2006) 352.
[6] A. Braem, et al., Nucl. Instr. and Meth. A 580 (2007) 1513;
A. Braem, et al., Nucl. Instr. and Meth. A 586 (2008) 300.
[7] I. Vilardi, et al., Nucl. Instr. and Meth. A 564 (2006) 506.
[8] Y. Shao, et al., IEEE Trans. Nucl. Sci. NS-49 (2002) 649.
[9] GEANT4.web.cern.ch;
S. Agostinelli, et al., Nucl. Instr. and Meth. A 506 (2003) 250;
M.G. Pia, Nucl. Phys. B Proc. Suppl. 125 (2003) 60.
[10] M. Moszynski, et al., Nucl. Instr. and Meth. A 484 (2002) 259.
[11] A. Levin, C. Moisan, A more physical approach to model the surface treatment of scintillation counters and its implementation into DETECT, in: Nuclear Science Symposium Record, 1996 IEEE, vol. 2, 1996, pp. 702–706.
[12] V.V. Nagarkar, et al., A high efficiency pixilated detector for small animal PET, University of California, Paper 178, 2004.
[13] K. Wienhard, et al., IEEE Trans. Nucl. Sci. NS-49 (2002) 104.